Modeling of Converter Losses with High Fidelity in a Physically Based Object-Oriented Way

Chiyang Zhong, *Student Member, IEEE*, A. P. Sakis Meliopoulos, *Fellow, IEEE*, Jingfan Sun, *Student Member, IEEE*,
Maryam Saeedifard, *Senior Member, IEEE*, Boqi Xie, *Student Member, IEEE*
School of Electrical and Computer Engineering, Georgia Institute of Technology, USA
Email: c.zhong@gatech.edu

Abstract—**Converters are a vital part of modern-day power systems. Converter losses are essential in determining the efficiency of power delivery. This paper presents a physically based modeling of converters for accurate evaluation of converter losses. It is a novel approach that can compute total losses for any type of converters with high fidelity as well as the distribution of losses among the various components of the converter. A standard modeling syntax is described in detail. Two example converters are constructed and their performance and losses are evaluated to demonstrate the usefulness of this modeling technique. Simulation results show that the method provides the total converter losses as well as the losses of each part of the converter components, making it an excellent tool for identifying the parts of a converter where most of losses occur. This information can be used for design optimization.**

Index Terms—**Converter Losses, High Fidelity, Object-Oriented, Physically Based Modeling.**

I. INTRODUCTION

Converters are widely used in modern-day power systems. To transfer power between AC and DC grids, AC-DC converters are essential. To convert voltage levels in DC circuits, DC-DC converters are used. As these systems transfer large amounts of energy, efficiency is a primary design concern. Determining the losses in the various components of a converter is a rather complex task. Yet, it is of great importance to be able to model converter losses and use this information to optimize designs. We present a novel modeling technique that can provide analysis of losses with high fidelity.

Most prior works model the losses of specific converters or they determine the efficiency of the converter experimentally. Reference [1] presents a forward-flyback converter design and its efficiency is evaluated. The forward converter and flyback converter efficiencies are also studied for comparison. A two-level back-to-back power converter model for wind applications with power losses simulated is presented in [2]. Simulation results show that a decrease in AC voltage amplitude induces a significant drop in overall converter efficiency. Reference [3] presents a fast steady-state model to calculate losses in modular multilevel converters (MMC). It is able to capture different sources of power losses in steady-state operation. Another MMC loss modeling technique is presented

in [4], where a semi-numerical method for loss calculation using the virtual submodule concept is proposed. It allows for a fast estimation of the submodule losses under different operating conditions, control schemes, and modulation methods. Modeling of AC buck converters is introduced in [5] that includes modeling and thermal analysis of different AC buck converter circuits. In [6], a dual-active bridge loss model is derived based on the identification of switching condition boundaries between hard-switching, partial zero-voltage-switching, and zero-voltage-switching.

This paper introduces an innovative physically based modeling (PBM) method for converter loss evaluation. In order to model losses accurately, converters must be modeled as detailed as possible. We use a physically based modeling approach. All circuits and components of the converter are modeled explicitly. For example, the electronic switch (IGBT, thyristor, etc.) is modeled with its on and off states, junction voltage, junction capacitance as well as supporting components, snubber circuits, diodes, etc. The implementation is object-oriented where each component is an object. Unlike existing literature of converter efficiency, our modeling approach is not confined to only one specific type of converters. Any converter topology with different electronic valves can be modeled with this tool. In fact, not just converters, any device can be modeled using this approach. The quadratized device model (QDM) and the algebraic quadratic companion form (AQCF) are the standard syntax used to achieve object orientation. The quadratic integration method is imbedded into the process of transforming the models from QDM to AQCF. It has been proven to be more accurate than other traditionally used methods for power system transient analysis, such as trapezoidal integration. At the same time, it exhibits better numerical stability properties [7]. The method is demonstrated with two example converters, an AC-DC converter and a DC-DC converter.

The paper is organized as follows. Section II introduces the PBM technique used for converter loss modeling. Section III describes how the AC-DC and DC-DC converters are constructed. Section IV describes the computations for converter losses and efficiency. A case study is presented in section V with sample simulation results. Section VI provides concluding remarks for the paper.

II. PHYSICALLY BASED MODELING

Device models are written as mathematical objects derived directly from the device physical circuits. By representing all details of the physical construction of the device, a high-fidelity model is achieved.

The physical ON and OFF models of IGBTs and thyristors are shown in Fig. 1. The parameters may be different between an IGBT and a thyristor, but they are both modeled as variable resistors with a voltage gap in parallel with a parasitic branch. In ON state, a forward voltage drop is present. With similar ratings and operating conditions, an IGBT has a larger forward voltage drop than a thyristor, thus creating more losses [8], [9]. Other power electronic switches can be similarly modeled.
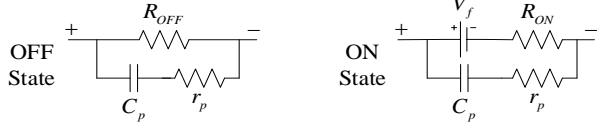
Figure 1. IGBT and thyristor ON and OFF physical models

Any other component of the converter can be modeled the same way. By combining the models of all components of the converter, the physically based model of the entire converter is obtained. We present the overall procedure and casting the model into an object form in the next section.

III. CONVERTER MODEL CONSTRUCTION

To construct the complicated converter models in high fidelity, we disassemble them into several smaller component models. All these components are first modeled individually using the PBM method, before being put together to form the overall converter models. In this paper, we consider the AC-DC and DC-DC converter models as shown in the upper and lower parts of Fig. 2, respectively. For illustration purposes, constructions of the IGBT valve and the transformer are described in details in the following subsections.
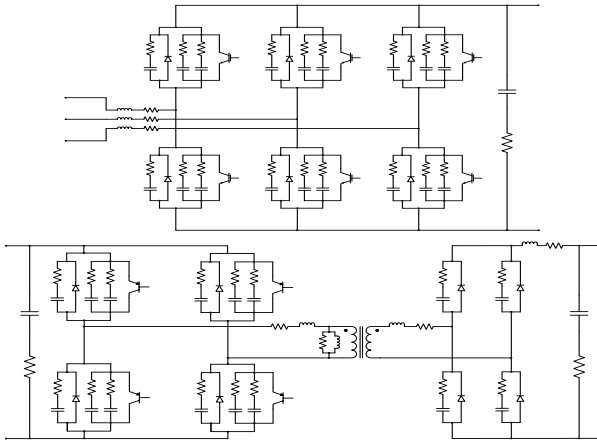
Figure 2. AC-DC and DC-DC converter models

A. IGBT Valve Model

Although each converter has more than one valves, each valve is modeled separately. A detailed valve model is shown in Fig. 3, with an ON and an OFF model to approximate the valve characteristics. The valve resistance R_v has different values under different conditions. The OFF resistance R_{vOFF} is

a very large value while the ON resistance R_{vON} is very small. A constant forward voltage drop V_f is associated with the ON status. In addition to a parasitic capacitance C_p and a parasitic resistance r_p, the valve model also includes a snubber circuit, which has a snubber capacitance C_s in series with a snubber resistance R_s. Note that for numerical stability as discussed in [10], the parasitic resistance and snubber resistance should satisfy $2r_p \geq \alpha h/C_p$ and $2r_s \geq \alpha h/C_s$, respectively, where h is the time step and α is the damping coefficient that has value between 0 and 1.
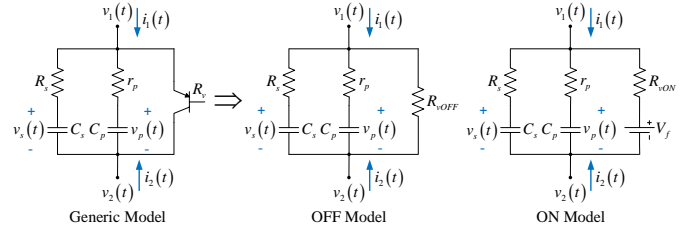
Figure 3. Detailed IGBT valve ON and OFF models

$$i_1(t) = \frac{1}{R_{vOFF}}\left(v_1(t) - v_2(t)\right) + C_p \frac{d}{dt} v_p(t) + C_s \frac{d}{dt} v_s(t)$$

$$i_2(t) = -\frac{1}{R_{vOFF}}\left(v_1(t) - v_2(t)\right) - C_p \frac{d}{dt} v_p(t) - C_s \frac{d}{dt} v_s(t)$$

$$0 = v_1(t) - v_2(t) - v_p(t) - r_p C_p \frac{d}{dt} v_p(t)$$

$$0 = v_1(t) - v_2(t) - v_s(t) - R_s C_s \frac{d}{dt} v_s(t) \quad (1)$$

The corresponding mathematical OFF model of a valve is presented in the QDM form as given in (1). For the ON model, only the first two equations in (1) are slightly modified, as shown in (2). The states variables of the IGBT valve model are $[v_1(t) \quad v_2(t) \quad v_p(t) \quad v_s(t)]^T$.

$$i_1(t) = \frac{1}{R_{vON}}\left(v_1(t) - v_2(t) - V_f\right) + C_p \frac{d}{dt} v_p(t) + C_s \frac{d}{dt} v_s(t)$$

$$i_2(t) = -\frac{1}{R_{vON}}\left(v_1(t) - v_2(t) - V_f\right) - C_p \frac{d}{dt} v_p(t) - C_s \frac{d}{dt} v_s(t) \quad (2)$$
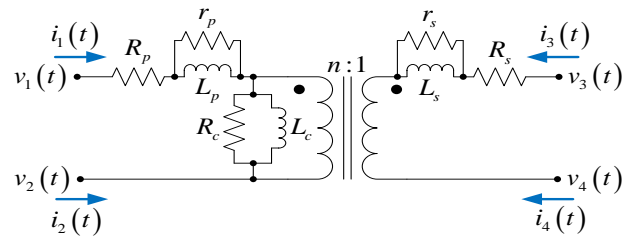
Figure 4. Detailed transformer model

B. Transformer Model

There exists a transformer in the DC-DC converter model to provide electrical isolation between the input and the output. The detailed transformer model is shown in Fig. 4. R_p and L_p are the resistance and inductance of the primary winding, respectively, while R_s and L_s are their counterparts on the secondary winding. The core resistance is R_c and the core inductance is L_c. For numerical stability, stabilizers $r_p =$

$4L_p/h$ and $r_s = 4L_s/h$ are added in parallel with L_p and L_s, respectively [10].

The transformer model has 7 state variables, given by $[v_1(t)\quad v_2(t)\quad v_3(t)\quad v_4(t)\quad i_p(t)\quad i_s(t)\quad i_c(t)]^T$ where $i_p(t)$, $i_s(t)$, and $i_c(t)$ are respectively the currents flowing through the primary, secondary, and core inductors. The mathematical representation of the transformer is as follows.

$$i_1(t) = i_p(t) + \frac{L_p}{r_p}\frac{d}{dt}i_p(t)$$

$$i_2(t) = -i_p(t) - \frac{L_p}{r_p}\frac{d}{dt}i_p(t)$$

$$i_3(t) = i_s(t) + \frac{L_s}{r_s}\frac{d}{dt}i_s(t)$$

$$i_4(t) = -i_s(t) - \frac{L_s}{r_s}\frac{d}{dt}i_s(t)$$

$$0 = v_1(t) - v_2(t) - R_p i_p(t) - \frac{R_p + r_p}{r_p}L_p\frac{d}{dt}i_p(t) - L_c\frac{d}{dt}i_c(t)$$

$$0 = v_3(t) - v_4(t) - R_s i_s(t) - \frac{R_s + r_s}{r_s}L_s\frac{d}{dt}i_s(t) - \frac{L_c}{n}\frac{d}{dt}i_c(t)$$

$$0 = i_p(t) + \frac{1}{n}i_s(t) - i_c(t) + \frac{L_p}{r_p}\frac{d}{dt}i_p(t) + \frac{L_s}{nr_s}\frac{d}{dt}i_s(t) - \frac{L_c}{R_c}\frac{d}{dt}i_c(t)$$

C. Quadratized Device Model

The qudratized device model (QDM) is an object-oriented syntax to represent the physical model. Any device can be modeled this way. A general form of the QDM is given by

$$i(t) = Y_{eqx1}\mathbf{x}(t) + D_{eqxd1}\frac{d\mathbf{x}(t)}{dt} + C_{eqc1}$$

$$0 = Y_{eqx2}\mathbf{x}(t) + D_{eqxd2}\frac{d\mathbf{x}(t)}{dt} + C_{eqc2} \tag{3}$$

$$0 = Y_{eqx3}\mathbf{x}(t) + \left\{ \mathbf{x}(t)^T \left\langle F_{eqxx3}^i \right\rangle \mathbf{x}(t) \right\} + C_{eqc3}$$

where $i(t)$ and $\mathbf{x}(t)$ are the terminal currents and state variables at time t, respectively. Matrices Y are coefficients to the linear terms, while matrices D are coefficients to the differential terms. Quadratic term coefficients are defined in matrices F and constant terms are stored in vectors C. As an example, the IGBT ON model in the above form is written as:

$$Y_{eqx1} = \begin{bmatrix} \frac{1}{R_{vON}} & -\frac{1}{R_{vON}} & 0 & 0 \\ -\frac{1}{R_{vON}} & \frac{1}{R_{vON}} & 0 & 0 \end{bmatrix}, \quad Y_{eqx2} = \begin{bmatrix} 1 & -1 & -1 & 0 \\ 1 & -1 & -1 & 0 \end{bmatrix}$$

$$D_{eqxd1} = \begin{bmatrix} 0 & 0 & C_p & C_s \\ 0 & 0 & -C_p & -C_s \end{bmatrix}, \quad D_{eqxd2} = \begin{bmatrix} 0 & 0 & -r_p C_p & 0 \\ 0 & 0 & 0 & -r_s C_s \end{bmatrix}$$

$$C_{eqc1} = \begin{bmatrix} -\frac{1}{R_{vON}}V_f \\ \frac{1}{R_{vON}}V_f \end{bmatrix}, \quad C_{eqc2} = 0, \quad Y_{eqx3} = 0, \quad F_{eqxx3} = 0, \quad C_{eqc3} = 0$$

D. Algebraic Quadratic Companion Form

For each device model written in the QDM form in (3), the quadratic integration method is applied to produce the algebraic quadratic companion form (AQCF) over time intervals $[t, t_m]$ and $[t, t + h]$, where $t_m = t + h/2$ and h is the time step [7]. The AQCF can be expressed as

$$\begin{cases} i(t) \\ 0 \\ 0 \\ i(t_m) \\ 0 \\ 0 \end{cases} = Y_{eqx}\mathbf{x}(t, t_m) + \left\{ \mathbf{x}(t, t_m)^T \left\langle F_{eqx}^i \right\rangle \mathbf{x}(t, t_m) \right\} + B_{eq} \tag{4}$$

$$B_{eq} = N_{eqx}\mathbf{x}(t-h) + M_{eq}i(t-h) + K_{eq}$$

where B_{eq} is called the past history vector, which stores the model information from the previous time step in simulations. Matrices Y_{eqx}, F_{eqx}, N_{eqx}, M_{eq}, and K_{eq} can be computed directly from the coefficient matrices in (3) as given in [11].

Besides the modeling of devices, this PBM standard syntax can also be used in other applications including state estimation, optimal control, contingency analysis, etc.

E. Overall Converter Models

After each component model is in the AQCF syntax, the component models can be combined to form the AQCF model for the entire converter. This process applies Kirchhoff's current law (KCL) at each node of the converter eliminating the through variables (terminal currents) of each component, and append all the internal equations of each component.

Different operating modes of a converter are defined and each mode corresponds to a set of ON/OFF diodes and IGBT valves. The operating mode is provided by a controller, which is modeled the same way with the standard syntax. Note that the AC-DC and DC-DC converters use different controllers.

IV. CONVERTER LOSS COMPUTATION

The instantaneous power loss of any device measured at time t is computed as

$$p_{loss}(t) = \sum_{i \in S} v_i(t)i_i(t) \tag{5}$$

where S is the set of terminals of the selected device, which are the device nodes connected to outside circuits. The AC-DC converter in Fig. 2 has 5 terminals, while the DC-DC converter has 4 terminals. Note that voltage v_i is the potential and current i_i is the current flowing into the device at node i. The average power losses over a certain time period T are given by

$$\bar{P}_{loss} = \frac{1}{T}\int_0^T p_{loss}(t)dt \tag{6}$$

The average input power $\bar{P}_{in}$ or output power $\bar{P}_{out}$ can be calculated the same way. In this case, S in equation (5) becomes the set of input or output nodes, respectively. The overall device losses averaged over a cycle presented as a percentage of the output power is given by $\bar{P}_{loss}/\bar{P}_{out} \times 100\%$. Because all states and all components of the inverter are represented, the loss computations can be performed not only
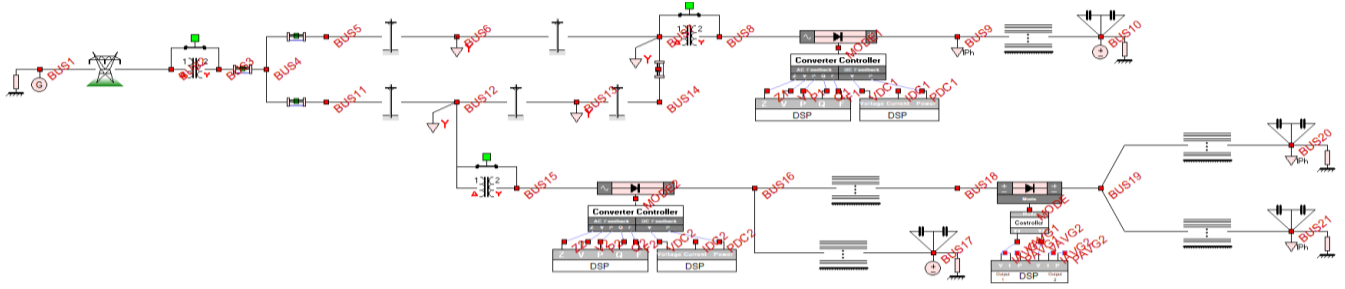
Figure 5.   Distribution system for case study

for the overall converter but also for any component of the converter, valves, snubber circuits, etc.

V.   CASE STUDY

This section shows a case study for evaluating converter losses, including analyses of converter component losses. Four cases with different loading conditions in the system are simulated in software WinIGS.

A. Test Case Setup

We constructed a hybrid distribution test system containing two AC-DC converters and one DC-DC converter, as shown in Fig. 5. A 30-MVA transformer is at BUS2, stepping down the voltage level from transmission 115 kV to distribution 13.8 kV. There are 4 three-phase balanced AC loads located at BUS6, BUS7, BUS12, and BUS13. Two 2-MVA transformers are used to step down the voltage from 13.8 kV to 480 V, each followed by a 50-kVA AC-DC converter. 13.8 kV AC is converted into 850 V DC at BUS9 and BUS16. A 30-kW DC-DC converter steps down the DC voltage to 200 V at BUS19, powering two DC loads at BUS20 and BUS21. Another DC load is at BUS9. BUS10 and BUS17 each has one DC source. The rated power consumptions of the loads are provided in Table I, which is viewed as 100% loading. Three other cases with 80%, 50%, and 30% loading are also simulated.

TABLE I.   RATED POWER CONSUMPTIONS OF LOADS

	BUS6	*BUS7*	*BUS12*	*BUS13*
AC Loads	500 kW 30 kVar	300 kW 30 kVar	400 kW 50 kVar	200 kW 20 kVar
DC Loads	*BUS9*	*BUS20*	*BUS21*	
	50 kW	10 kW	10 kW	

Each converter is controlled by its own controller, which receives measurement data from DSP modules for feedback control. Both AC-DC converters use a P-Q control scheme, which control the real and reactive power outputs P_{AC} and Q_{AC} at the AC side, while the DC-DC converter only controls the output voltage V_{OUT}. The reference values set in the controllers for the 100% loading case are provided as follows. For AC-DC converter 1 at BUS 8, $P_{AC} = 40$ kW and $Q_{AC} = 10$ kVar. For AC-DC converter 2 at BUS15, P_{AC} and Q_{AC} are set to be -20 kW and -10 kVar, respectively. The DC-DC converter has its output voltage V_{OUT} set to 200 V. Note that negative power values represent the absorption of power at the AC sides of the AC-DC converters. Hence, AC-DC converter 1 works as an inverter and AC-DC converter 2 is a rectifier. These power setpoints are changed proportionally according to the percentage of loading for the other loading conditions.

The switching frequency for all three converters is 5000 Hz and the simulation time step used is 1 µs. Due to limited space, we will not provide all the parameters used in the simulation. However, some major converter parameters are listed in Table II. The parameters of the IGBT valve are obtained from datasheets [8], while the transformer parameters are taken from [12]. The notations used in the table are the same as those shown in Figs. 3 and 4.

TABLE II.   IGBT VALVE AND TRANSFORMER PARAMETERS

Component	Parameters			
IGBT Valve	R_{vON}	30 mΩ	R_{vOFF}	1000 kΩ
	C_p	87 pF	C_s	174 pF
	r_p	2.874 kΩ	r_s	1.437 kΩ
	V_f	1.6 V		
Transformer	R_p	43 mΩ	R_s	10.75 mΩ
	L_p	6.75 µH	L_s	1.6875 µH
	r_p	27 Ω	r_s	6.75 Ω
	R_c	300 kΩ	L_c	8 mH
	n	2		

In order to compare the PBM case with a baseline case, the three converters in Fig. 5 were simulated in Matlab/Simulink. We modeled the converters with the same parameters, controls, feedback and voltage levels used in the case study.

TABLE III.   CONVERTER AND COMPONENT LOSSES IN DIFFERENT CASES

	100% Loading	80% Loading	50% Loading	30% Loading
AC-DC Converter 1	1.942 %	1.666 %	1.364 %	1.290 %
AC-DC Converter 2	3.588 %	2.848 %	1.937 %	1.225 %
DC-DC Converter	5.705 %	4.287 %	4.143 %	4.075 %
IGBT Valve	0.164 %	0.149 %	0.118 %	0.110 %
Snubber Circuit	0.000515 %	0.000704 %	0.001115 %	0.001847 %

B. Simulation Results

Four cases with 100%, 80%, 50%, and 30% loading respectively are simulated. The results are presented in Table III. Overall losses of the three converters under different loading conditions are given. In addition, losses at one IGBT valve in AC-DC converter 1 and the corresponding snubber circuit are presented. Note that all the losses are computed in

steady state operation and they are the average losses over one cycle, expressed in percentage of the converter output powers.

From Table III, it can be noticed the losses drop for all three converters and the IGBT valve as the amount of loading decreases. These results make sense because with the converter output voltages kept around 850 V either by distribution generators or voltage control, the currents through the converters decrease when the loading is reduced, thus inducing losses. The IGBT valve monitored has less current flowing through as a result, so its losses have also dropped. Notice that the total losses of all the valves are more than half of the overall converter losses. As for the snubber circuit, the percentage of losses has increased during the loss of loads. Since snubber circuits almost draw no current during converter operation, the decrease of converter current in less loading cases does not affect it much. Hence, the snubber circuit losses have accounted for a higher percentage in these cases.
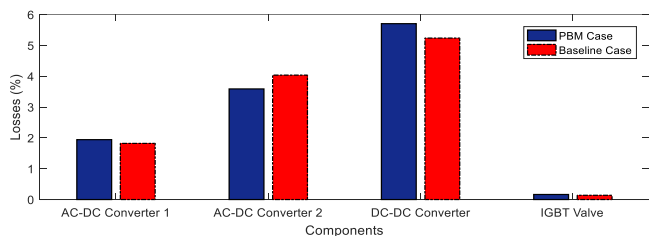

Figure 6.   Loss comparisons of two cases under 100% loading condition

Loss comparisons between the PBM and the baseline cases under the 100% loading condition are illustrated in Fig. 6, which clearly shows that our modeling technique gives similar loss results as that given by Simulink. Small differences exist as Simulink models the devices in less detail than our approach. Note that the snubber circuit is not compared here because in Simulink it is encased in the IGBT block and its losses cannot be separated. The advantage of our modeling method is that it can model all the details of the converter and compute the losses in each part using the actual current and voltage waveforms in each part of a converter.
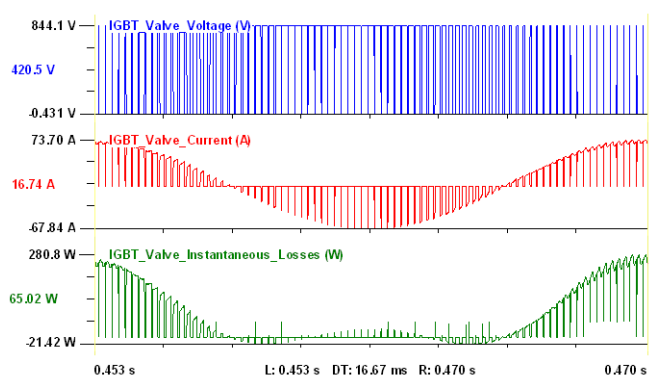

Figure 7.   IGBT valve losses under 100% loading condition

For illustration of the loss computation method, Fig. 7 shows the voltage across the IGBT (first trace), the current through the IGBT (second trace), and the instantaneous power (third trace) consumed by the IGBT over one cycle under 100% loading condition. The average value of the third trace is the average consumed losses in the IGBT, which is 65.02 W as shown on the left side of the plot.

VI.   CONCLUSIONS

This paper introduces a physically based modeling approach for computing converter losses with high-fidelity as well as losses in each component of a converter. An object-oriented implementation of this method has been presented. Two example AC-DC and DC-DC converters are used to demonstrate the method. The method is applicable to any converter topology and power electronic switch technology.

A test case is presented to illustrate the performance of the example converter loss modeling technique under various loading conditions. The simulation results show that the converter total loss and efficiency can be accurately evaluated as well as the losses at each component of the converter. This knowledge is useful in the process of optimizing converter designs. In addition, comparisons are made between the results with the propose method and a baseline case. The differences are minor.

We presently use this method to compare efficiencies of hybrid systems (AC and DC systems linked by converters) to determine the best designs for hybrid systems.

REFERENCES

[1] M. A. K. A. Biabani, "Simulation, mathematical calculation and comparison of power factor and efficiency for forward, fly back and proposed forward-flyback converter," in *Proc. Intl. Conf. on Electrical, Electronics, and Optimization Techniques (ICEEOT)*, Chennai, 2016.

[2] I. Mrčela, D. Sumina, F. Sačić, and T. Bariša, "A wind turbine two level back-to-back converter power loss study," in *Proc. IEEE Intl. Power Electronics and Motion Control Conference (PEMC)*, Varna, 2016.

[3] S. Rodrigues, A. Papadopoulos, E. Kontos, T. Todorcevic, and P. Bauer, "Steady-State Loss Model of Half-Bridge Modular Multilevel Converters," *IEEE Trans. Industry Applications*, vol. 52, no. 3, pp. 2415-2425, May 2016.

[4] A. Christe and D. Dujic, "Virtual Submodule Concept for Fast Semi-Numerical Modular Multilevel Converter Loss Estimation," *IEEE Trans. Industrial Electronics*, vol. 64, no. 7, pp. 5286-5294, July 2017.

[5] R. L. Gorbunov, I. A. Kalinowski, and G. I. Poskonnyy, "Power losses and thermal modeling of AC Buck converters," in *Proc. 16th Intl. Conf. of Young Specialists on Micro/Nanotech. and Electron Devices,* 2015.

[6] L. Xue, D. Boroyevich, and P. Mattavelli, "Switching condition and loss modeling of GaN-based dual active bridge converter for PHEV charger," in *Proc. IEEE Applied Power Electronics Conf. and Expo. (APEC)*, Long Beach, CA, 2016.

[7] A. P. Meliopoulos, G. J. Cokkinides, and G. K. Stefopoulos, "Quadratic integration method," in *Proc. Intl. Conf. Power System Transients (IPST)*, Montreal, Canada, June 2005.

[8] *Resonant Switching Series IHW40N120R3*, Rev. 2.2, Infineon Technologies, 2015.

[9] *Teccor brand Thyristors SK255KD*, Littelfuse, 2015.

[10] W. Gao, E. Solodovnik, R. Dougal, G. Cokkinides, and A. P. S. Meliopoulos, "Elimination of numerical oscillations in power system dynamic simulation," in *Proc. Applied Power Electronics Conf. and Expo.*, pp. 790-794, Feb. 2003.

[11] L. Sun, R. Fan, A. P. S. Meliopoulos, Y. Liu, and Z. Tan, "Capacitor bank protection via constraint WLS dynamic state estimation method (CWLS-DSE)," in *Proc. North American Power Symp. (NAPS)*, Denver, CO, 2016.

[12] L. F. Costa, G. Buticchi, and M. Liserre, "Highly Efficient and Reliable SiC-Based DC–DC Converter for Smart Transformer," *IEEE Trans. Industrial Electronics*, vol. 64, no. 10, pp. 8383-8392, Oct. 2017.

[13] S. Helland, "Evaluation of a Medium-Voltage High-Power Bidirectional Dual Active Bridge DC/DC Converter for Marine Applications," Master thesis, Dept. of Electric Power Eng., Norwegian University of Science and Technology, 2017.